Phonon focusing in superlattices

1998 J. Phys.: Condens. Matter 10 8787

(http://iopscience.iop.org/0953-8984/10/39/015)

J. Phys.: Condens. Matter **10** (1998) 8787–8798. Printed in the UK PII: S0953-8984(98)94537-4

Phonon focusing in superlattices

Yukihiro Tanaka, Michiko Narita and Shin-ichiro Tamura
Department of Applied Physics, Hokkaido University, Sapporo 060, Japan

Received 26 May 1998, in final form 20 July 1998

Abstract. Phonon focusing in periodic superlattices is studied in terms of the plane-wave expansion method rather than the conventional transfer matrix method. At the frequencies where the intramode and intermode Bragg reflections of phonons occur the group velocity of phonons along the growth direction vanishes, giving rise to the disappearance and/or appearance of phonon caustics. This can be explicitly shown by plotting theoretical phonon images in the planes both normal and perpendicular to the growth direction. Numerical examples are given for (001)GaAs/AlAs superlattices.

1. Introduction

The energy transport associated with lattice vibrations is governed by the group velocity of acoustic phonons. The spatial distribution of the phonon group velocities in a crystalline solid is highly anisotropic and the focusing and defocusing of ballistically propagating phonons have been observed experimentally [1]. The phonon imaging method reveals vividly how acoustic energy emanating from a point source is distributed in a crystal lattice [2]. In synthetic superlattices the zone folding effect due to the periodicity along the growth direction considerably modifies the phonon dispersion relations from those in bulk materials [3]. Specifically, the frequency gaps appear at the centre and boundaries of the folded Brillouin zone originating from intramode Bragg reflections at phonon wavelengths much longer than the lattice spacing. In addition, the existence of three phonon polarizations and their couplings induce the intrazone frequency gaps which are attributed to intermode Bragg reflections [4–6]. As a result, phonon group velocities and the resulting acoustic energy transport are expected to be highly frequency dependent and to exhibit quite different characteristics from bulk solids even in a low-energy region.

Recently, acoustic phonon propagation in multilayered systems has been a subject of considerable attention. Anomalous reductions of lattice thermal conductivity in semiconducting superlattices have been observed for a wide range of temperatures [7] and it is suggested that the modification of the phonon group velocity in the multilayered system plays an essential role for this phenomenon [8]. Also the thermal conductivity in the ferroelectric KDP sample in a multidomained state has been measured. The mode-dependent scattering of phonons from the 'internal' interfaces, i.e. domain walls, is considered to be the origin of the observed decrease in thermal conductivity [9, 10].

The purpose of the present work is to elucidate theoretically the ballistic phonon propagation in periodic superlattices. In particular, we consider how the intramode and intermode Bragg reflections affect the acoustic energy transport in superlattices. Thus, we concentrate our attention on the spatial distribution of phonons emitted from a point source. The results are presented by displaying theoretical phonon images (spatial maps

0953-8984/98/398787+12$19.50

of the phonon group velocities) in the planes both normal and perpendicular to the growth direction of superlattices.

Here, it should be noted that phonon imaging experiments with periodic superlattices InGaAs/AlAs and GaAs/AlAs were conducted several years ago [5, 6] to verify the predicted internal gaps in phonon dispersion relations associated with intermode phonon Bragg reflections [4]. In these experiments the acoustic energy or group velocities of phonons transmitted through *thin* (typically 3 μm) periodic superlattices deposited on a thick GaAs substrate (400 μm) were measured. Thus, the group-velocity distributions in the images observed are essentially those in the *substrate* material (GaAs) which is much thicker than the superlattice deposited on it [11, 12]. No information is obtained about group-velocity distribution inside the GaAs/AlAs superlattice because the superlattice is very thin.

The major role of the superlattices in those experiments is just to filter out the phonons within certain frequency windows, i.e. phonon stop bands. The existence of the phonon stop bands is recognized in the images as sharp reductions of transmitted phonon intensity with spatially anisotropic shapes. These shapes are frequency dependent but the background phonon image (phonon focusing in the GaAs substrate) is not altered even when the phonon frequency is changed in the sub-THz region. In contrast, the present study deals with the energy transport of phonons inside the superlattice itself and makes it clear how the phonons propagate in a superlattice across the layer interfaces. The predicted phonon images (phonon focusing patterns) or the group-velocity distributions of phonons in the GaAs/AlAs superlattice are changed quite markedly depending on frequency even in the sub-THz region, leading to the appearance or disappearance of phonon caustics. The validity of our predictions will be verified by phonon transmission or imaging experiments with a superlattice alone or with a superlattice and a substrate where the superlattice is much thicker than the substrate.

2. Formulation

We consider the system consisting of an infinite repetition of alternating layers of materials A (with thickness d_A, mass density ρ_A and elastic stiffness tensor c_A^{ijmn}) and B (with thickness d_B, mass density ρ_B and elastic stiffness tensor c_B^{ijmn}). The interfaces are parallel to the $\boldsymbol{x}_\parallel = (x, y) = (x_1, x_2)$ plane, with the z axis (x_3 axis) normal to the interfaces (see figure 1). Both A and B materials are cubic crystals and elastic anisotropy is taken into account. The equation governing the motion of lattice displacement $\boldsymbol{u}(\boldsymbol{r},\ t)$ of the system is given by

$$\rho(z)\ddot{u}_i = \partial_j[c_{ijmn}(z)\partial_n u_m] \qquad (i = 1, 2, 3) \tag{1}$$

where $\boldsymbol{r} = (\boldsymbol{x}_\parallel, z)$, $\rho(z)$ and $c_{ijmn}(z)$ are the position-dependent mass density and elastic stiffness tensor, and the summation convention over repeated indices is assumed. Usually, equation (1) is solved with a transfer matrix which connects the vibrational amplitudes of adjacent layers [6]. In the present work we use the Fourier expansion method to solve equation (1)

$$\boldsymbol{u}(\boldsymbol{r}, t) = \mathrm{e}^{\mathrm{i}(\boldsymbol{k}_\parallel \cdot \boldsymbol{x}_\parallel - \omega t)} \sum_\ell \mathrm{e}^{\mathrm{i}(k_z + G_\ell)z} \boldsymbol{a}_\ell \tag{2}$$

$$\rho(z) = \sum_\ell \mathrm{e}^{\mathrm{i}G_\ell z} \rho_\ell \tag{3}$$

$$c_{ijmn}(z) = \sum_\ell \mathrm{e}^{\mathrm{i}G_\ell z} c_\ell^{ijmn} \tag{4}$$

where $\boldsymbol{k} \equiv (\boldsymbol{k}_\parallel, k_z)$ is the wavevector, $G_\ell = 2\pi\ell/D$ with ℓ an integer and $D = d_A + d_B$ is the periodicity. The Floquet theorem required for a one-dimensional periodic system is satisfied by $\boldsymbol{u}$ given above and the Fourier coefficients take the form

$$f_0 = (F_A d_A + F_B d_B)/D \tag{5}$$

$$f_\ell = (F_A - F_B)\frac{1 - \mathrm{e}^{-2\pi\mathrm{i}\ell d_A/D}}{2\pi\mathrm{i}\ell} \qquad (\ell \neq 0) \tag{6}$$

where $f_\ell = (\rho_\ell, c_\ell^{ijmn})$, $F_I = (\rho_I, c_I^{ijmn})$ with $I = A$ and B, and f_ℓ should be replaced by $f_{2\ell} = 0$ and $f_{2\ell+1} = (F_A - F_B)/(2\ell + 1)\pi\mathrm{i}$ if $d_A = d_B$.

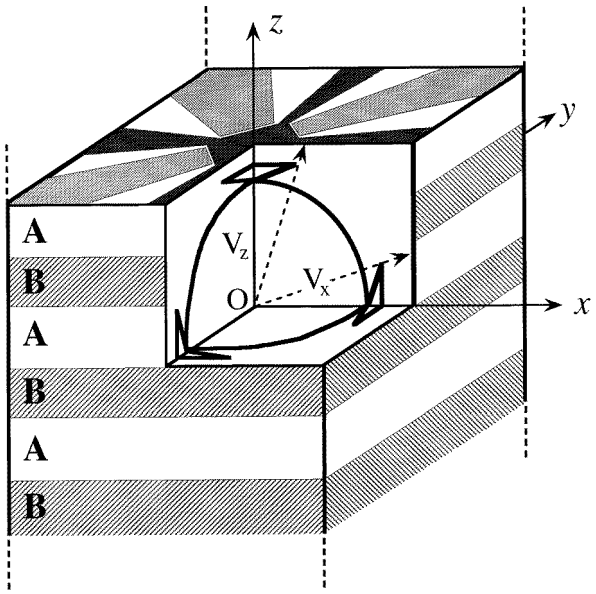

Figure 1. A periodic superlattice consisting of alternate *A* and *B* layers. The layer interfaces are parallel to the *x*–*y* plane and the growth direction is parallel to the *z* axis. The solid lines in the *x*–*y*, *y*–*z* and *z*–*x* sections illustrate the group-velocity curves of the slow transverse phonons and dashed lines with arrows indicate caustic directions. The phonon image on the *x*–*y* plane is shown schematically.

Substituting equations (2) to (4) into (1), we obtain an eigenvalue equation

$$\sum_n (\omega^2 \tilde{\rho}_{m,n} - \tilde{M}_{m,n})\boldsymbol{a}_n = 0 \qquad (m = 0, \pm 1, \pm 2, \ldots) \tag{7}$$

where $\tilde{\rho}_{m,n}$ and $\tilde{M}_{m,n}$ for given m and n are 3×3 matrices and their elements are

$$(\tilde{\rho}_{m,n})_{ij} = \rho_{m-n}\delta_{ij} \tag{8}$$

$$(\tilde{M}_{m,n})_{11} = C^{11}_{m-n}k_x^2 + C^{44}_{m-n}[k_y^2 + (k_z + G_m)(k_z + G_n)] \tag{9}$$

$$(\tilde{M}_{m,n})_{12} = (\tilde{M}_{m,n})_{21} = (C^{12}_{m-n} + C^{44}_{m-n})k_x k_y \tag{10}$$

$$(\tilde{M}_{m,n})_{13} = C^{12}_{m-n}k_x(k_z + G_n) + C^{44}_{m-n}k_x(k_z + G_m) \tag{11}$$

$$(\tilde{M}_{m,n})_{22} = C^{11}_{m-n}k_y^2 + C^{44}_{m-n}[k_x^2 + (k_z + G_m)(k_z + G_n)] \tag{12}$$

$$(\tilde{M}_{m,n})_{23} = C^{12}_{m-n}k_y(k_z + G_n) + C^{44}_{m-n}k_y(k_z + G_m) \tag{13}$$

$$(\tilde{M}_{m,n})_{31} = C^{12}_{m-n}k_x(k_z + G_m) + C^{44}_{m-n}k_x(k_z + G_n) \tag{14}$$

$$(\tilde{M}_{m,n})_{32} = C^{12}_{m-n}k_y(k_z + G_m) + C^{44}_{m-n}k_y(k_z + G_n) \tag{15}$$

$$(\tilde{M}_{m,n})_{33} = C^{11}_{m-n}(k_z + G_m)(k_z + G_n) + C^{44}_{m-n}(k_x^2 + k_y^2). \tag{16}$$

In the above equations (8)–(16), C^{ij}_{ℓ} are the Fourier coefficients of the elastic constants $C^{ij}(z)$ which are related to $c^{ijmn}(z)$ in the usual way. Thus, the frequencies and eigenvectors of phonons in a superlattice are obtained by solving equation (7). The expression for the group velocity $\boldsymbol{V}$ of phonons is also derived from equation (7). The result is

$$\boldsymbol{V} = \frac{\partial\omega}{\partial\boldsymbol{k}} = \frac{\sum_{m,n}(\boldsymbol{a}^t_m)^* \frac{\partial\tilde{M}_{m,n}}{\partial\boldsymbol{k}}\boldsymbol{a}_n}{2\omega\sum_{m,n}(\boldsymbol{a}^t_m)^*\tilde{\rho}_{m,n}\boldsymbol{a}_n} \tag{17}$$

where the superscript t means the transposition.

The periodicity along the growth direction of a superlattice induces the folding of the dispersion curves of phonons into a mini Brillouin zone of the size $k_z = 2\pi/D$. At the centre ($k_z = 0$) and boundaries ($k_z = \pm\pi/D$) of this folded Brillouin zone, the phonon dispersion curves are flat, i.e. $\partial\omega/\partial k_z = 0$, implying that the group velocity of phonons is parallel to the layer interfaces and no energy propagation along the growth direction of superlattices is allowed.

3. Numerical results

We present the numerical results for periodic (001) GaAs/AlAs superlattices with the same thickness of constituent layers, i.e. $d_A = d_B$ [13]. Figure 2 shows the dispersion relations of phonons propagating both normally and obliquely to the layer interfaces. The number of plane waves kept in the expansions (2) to (4) is seven, i.e. $\ell = -3$ to 3. The convergence has been checked by the fact that the dispersion curves calculated do not change at all even if we increase the number further. We also confirmed that the dispersion curves obtained are identical to the ones previously obtained with the transfer-matrix method [4–6]. This means that the Gibbs phenomenon characteristic of the Fourier-series expansion does not cause any inaccuracy of the calculations.

Here we note that, for the oblique case, the propagation direction (wavevector direction) of the longitudinal (L) mode in the GaAs layer is $\theta = 30^\circ$ rotated from the growth direction in the (010) plane. For the normal propagation two transverse (T) branches are degenerate and the frequency gaps are found only at the edges and centre of the folded Brillouin zone. For the oblique propagation the T phonons are split into fast transverse (FT) and slow transverse (ST) phonons, and an intrazone frequency gap in addition to the zone edge and zone centre gaps occurs due to the coupling of the different phonon polarizations (the L and ST phonons in the present case). Note that no intrazone gap is found for the normal propagation because of the decoupling of three phonon polarizations.

In the following we consider three typical frequencies $\omega D/v_0 = 2$, 3.2 and 4.1 ($v_0 = (C^{44}_{\mathrm{GaAs}}/\rho_{\mathrm{GaAs}})^{1/2} = 3.33 \times 10^5$ cm s^{-1}). The lowest frequency ($\omega D/v_0 = 2$) is in the frequency bands for three polarizations and the corresponding wavelengths are much longer than the unit period D. The second one ($\omega D/v_0 = 3.2$) is at the edge of the lowest frequency gap of the T mode for the normal propagation but this frequency is found inside the gap of the ST mode for a finite range of propagation angles oblique to the interface. The third one ($\omega D/v_0 = 4.1$) is close to the frequency at which the dispersion curves of the L and folded ST branches intersect at normal propagation. For a certain range of

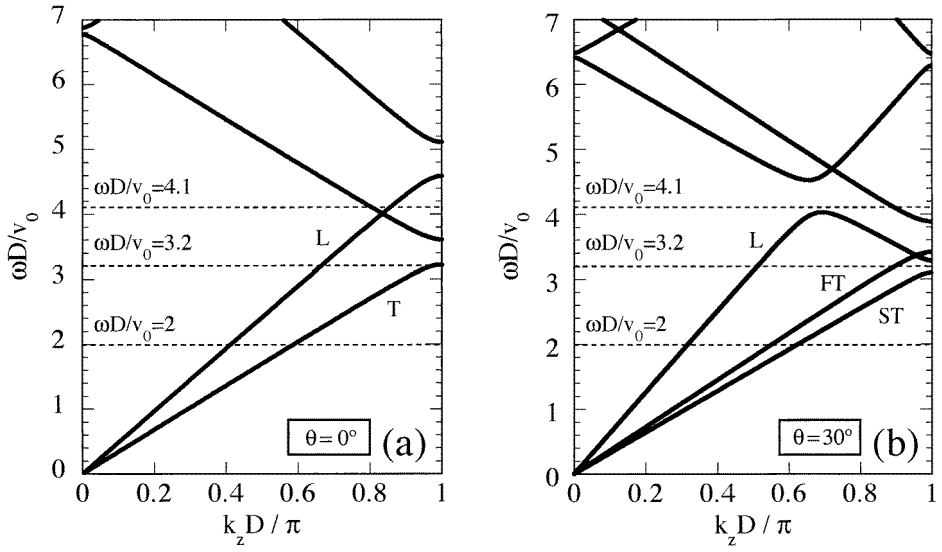

Figure 2. Dispersion relations of phonons in the periodic (001) GaAs/AlAs superlattice with equal thicknesses of layers. The propagation direction (wavevector direction) of the longitudinal (L) mode in the GaAs layer is inside the (010) plane and (*a*) $\theta = 0^\circ$ (normal to the interfaces) and (*b*) $\theta = 30^\circ$ rotated from the growth direction. The propagation angles of two transverse (T) modes (fast transverse (FT) and slow transverse (ST)) are determined from the conservation of $\boldsymbol{k}_\parallel$.

propagation angles this frequency is found inside the intrazone frequency gap due to the intermode Bragg reflection between the L and ST modes.

3.1. $\omega D/v_0 = 2$

At this frequency the constant-frequency surfaces (ω surfaces or slowness surfaces) of three phonon modes are entirely located inside the folded Brillouin zone and their sections in the (010) plane and the corresponding sections of the group-velocity surfaces are shown in figures 3(*a*) and 3(*b*), respectively. The ω curves (the sections of ω surfaces) of three phonon modes are deformed from circles due to the elastic anisotropy of the system. The folding of the group-velocity curves of the ST mode at the points A and B arises from the presence of the inflection points A and B in the ω curve which separate the convex region from the concave region. Here, it should be noted that additional group-velocity curves not shown in figure 3(*b*) exist in the (010) plane. They originate from the phonons with wavevectors out of the (010) plane but with the group-velocity vectors parallel to this plane. This means that the group-velocity surfaces in anisotropic, elastic media are multivalued in general.

The images of phonons in the x–y and y–z planes are shown in figures 3(c) and 3(d). These images span $-1 < x/L, y/L, z/L < 1$, where L is the length between the phonon source and the imaging plane and the brightness measures the relative phonon intensity. We note that the images are valid for $L \gg D$ because we assume perfect periodicity of the superlattice.

At this given frequency the wavelengths of the three modes of phonons are much longer than the unit period D and hence the phonons are essentially those in the bulk crystal with

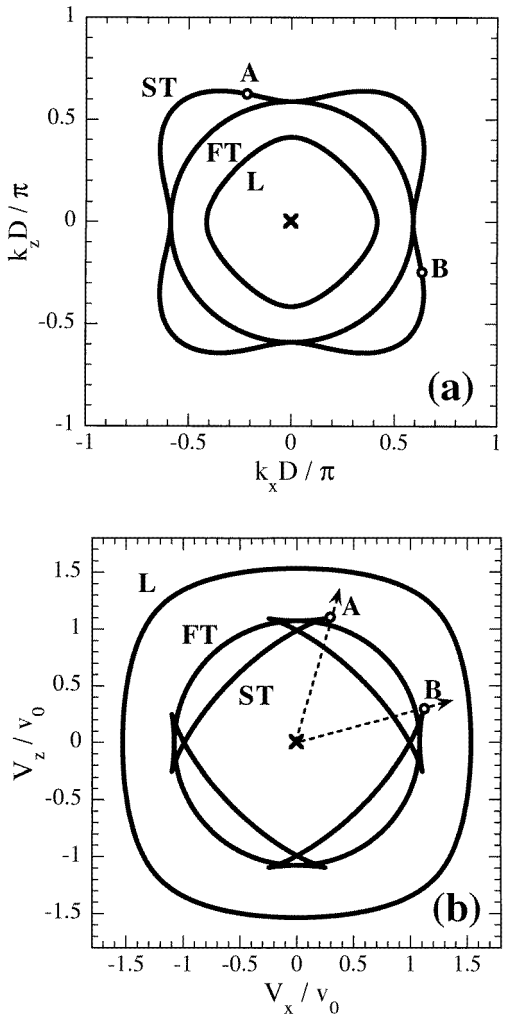

Figure 3. The results for $\omega D/v_0 = 2$. (a) The sections by the (010) plane of the constant-frequency surfaces of the longitudinal (L), fast transverse (FT) and slow transverse (ST) phonons. (b) Group-velocity curves corresponding to the phonons in the constant-frequency curves shown in (a). (c) Phonon image in the plane parallel to the layer interfaces (the x–y plane). (d) Phonon image in the plane normal to the layer interfaces (the y–z plane). The points labelled A and B correspond to the inflection points on the constant-frequency curve of the ST mode, giving rise to the foldings (caustics) in the group-velocity curve and the boundary points of the strong focusing regions in the images.

the mass density and elastic constants averaged over constituent materials. We find no particular difference between the phonon images in the planes parallel (x–y plane) and normal (y–z plane) to the interfaces. Both images are characterized by the box structures at the centre (due to the ST phonons), the narrow focusing regions extending both vertically and horizontally (due to the FT phonons) and the diagonal focusing structures with cuspidal structures around $(x/L, y/L) = (\pm 0.7, \pm 0.7)$ (due to the ST phonons). As expected, these

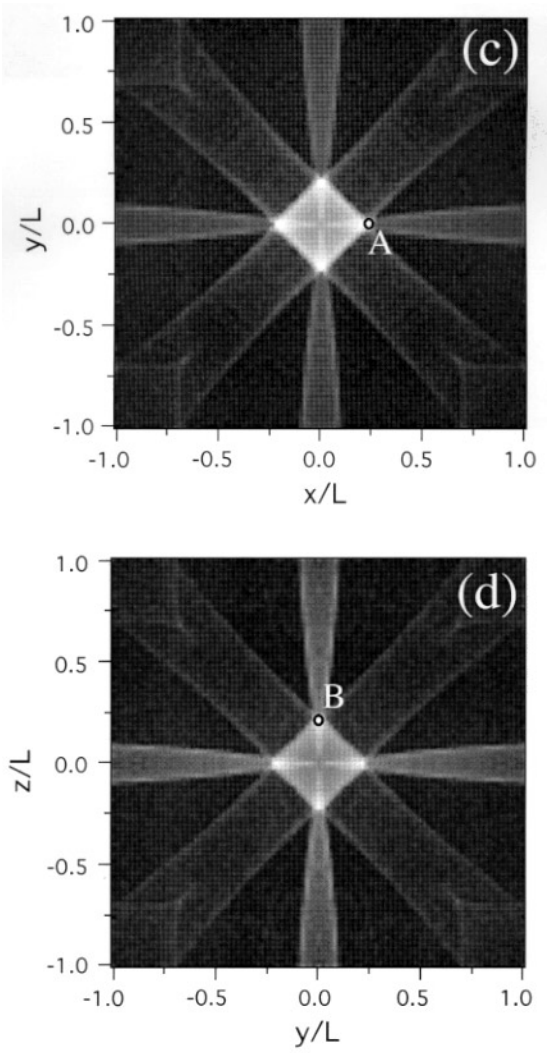

Figure 3. Continued

phonon-focusing characteristics are very similar to those of bulk GaAs published in the literature [11, 12].

3.2. $\omega D/v_0 = 3.2$

The (010) sections of the constant-frequency and the corresponding group-velocity curves are shown in figures 4(a) and 4(b), respectively. At this frequency certain portions of the ω curve (including several inflection points) of the outermost ST branch are removed from the Brillouin zone. This is due to the occurrence of the frequency gap at the folded zone boundary for a finite range of the propagation direction (see figure 2(b)). This also brings the caustics of the slow transverse mode near the growth direction (the V_z axis) into the frequency gap. Here it is important to note that at the points where the slowness curve intersects the boundaries of the Brillouin zone, the z component of the normal vector of this

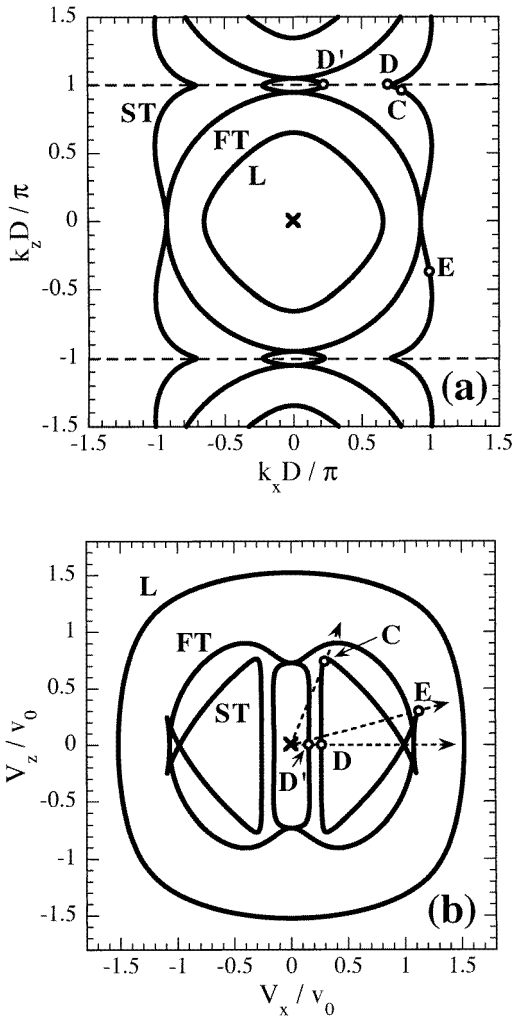

Figure 4. The results for $\omega D/v_0 = 3.2$. (a) The sections by the (010) plane of the constant-frequency surfaces of the longitudinal (L), fast transverse (FT) and slow transverse (ST) phonons. Dashed lines are the boundaries between the first and second Brillouin zones. (b) Group-velocity curves corresponding to the constant-frequency curves shown in (a). (c) Phonon image in the plane parallel to the layer interfaces (the x–y plane). Several corresponding points on the constant-frequency and group-velocity curves are labelled, C, D, D′ and E.

curve vanishes, implying that $V_z = 0$. Thus, the group-velocity curve of the ST mode near the V_z axis bends markedly towards the V_x axis as shown in figure 4(b) (points D and D′) and the ST caustics (those corresponding to point A in figure 3) disappear from the curve.

As a result, the box structure of high phonon intensity at the centre of the x–y plane image, which is characteristic of low frequencies (see figure 3(c)), cannot be seen in figure 4(c). However, almost no change is recognized in the image in the y–z plane (hence it is not shown here) as can be expected from the similarity of the large V_x parts of the group-velocity curves shown in figures 3(b) and 4(b).

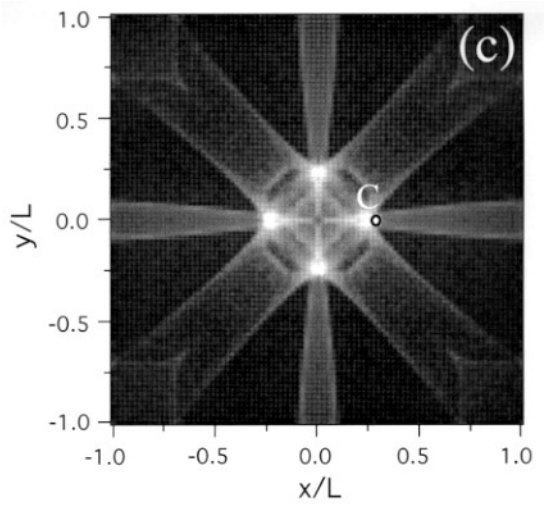

Figure 4. Continued

3.3. $\omega D/v_0 = 4.1$

The (010) sections of the ω curves and the corresponding group-velocity curves are shown in figures 5(a) and 5(b). The structures of both kinds of curves are much more complicated than those of the previous cases. An interesting feature is the coalescence of the innermost curve of the L mode and the one folded from the outermost ST curve (at the points close to F and G, for instance), which induces the gap (absence of the branch around these points) physically interpreted as an intermode Bragg reflection. The existence of this gap forces the group-velocity curves of the L and ST modes to deform again towards $V_z = 0$. This effect produces the foldings of the group-velocity curves of L and ST modes, leading to the occurrence of the caustics at the points F and G. At the same time the caustics at H and J occur due to the intramode Bragg reflections of transverse phonons.

A remarkable feature of these effects is seen in the phonon images shown in figure 5(c) (plotted for the slightly expanded region $-1.2 < x/L, y/L < 1.2$) and figure 5(d) (plotted for the region $-1 < y/L, z/L < 1$). In the image of the x–y plane a new circular caustic (passing through the point G) of the L mode of radius about $\sim L$ can be seen. This caustic is also recognized in the image of the y–z plane. Also in the y–z plane we find the truncation of the vertical FT focusing regions at about $z/L = 0.8$ (at the point H close to G).

4. Concluding remarks

In the present work we have studied the phonon focusing in a periodic superlattice consisting of alternating GaAs and AlAs layers. The Brillouin-zone folding characteristic of an artificially periodic system leads to the occurrence of zone-centre, zone-edge and internal gaps in the phonon dispersion relations at frequencies much lower than those of the bulk materials. These frequency gaps affect considerably the acoustic energy propagation in superlattices. Specifically, the disappearance and/or appearance of phonon caustics is found. The effects are entirely caused by the periodicity of the layering system and hence are more conspicuous in the direction perpendicular to the layer interfaces than that parallel to the interfaces. These new predictions should be verified by a phonon transmission experiment

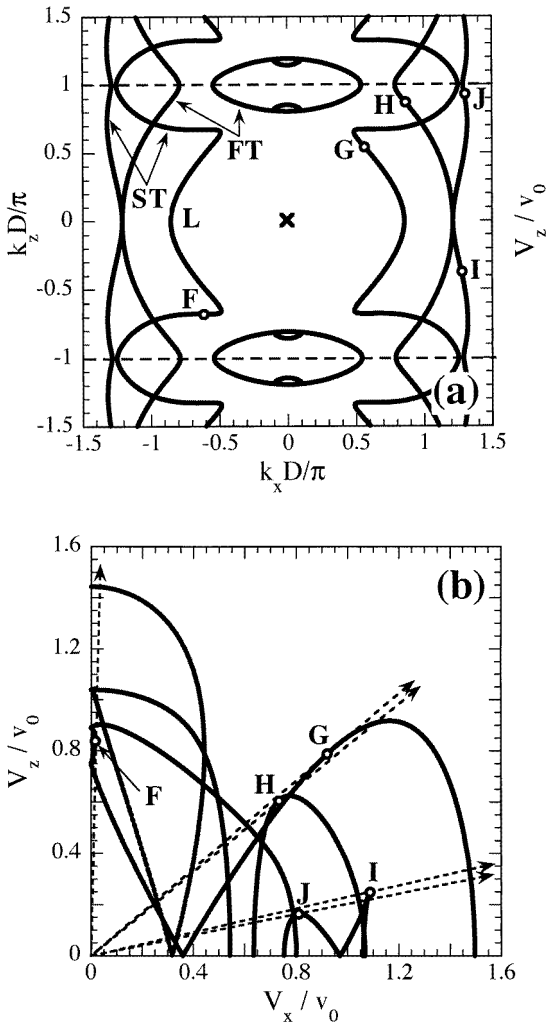

Figure 5. The results for $\omega D/v_0 = 4.1$. (a) The sections by the (010) plane of the constant-frequency surfaces of the longitudinal (L), fast transverse (FT), and slow transverse (ST) phonons. (b) Group-velocity curves corresponding to the constant-frequency curves shown in (a). The curves in the first quadrant are shown. (c) Phonon image in the plane parallel to the layer interfaces (the x–y plane). The inset shows a magnification of the centre of the image. (d) Phonon image in the plane normal to the layer interfaces (the y–z plane). The inset shows a magnification of the rectangular region at the corner of the box structure. Several corresponding points on the constant-frequency and group-velocity curves are labelled, F, G, H, I and J.

with a thick periodic superlattice in which the angular dependence of the ballistic phonon propagation inside the superlattice may be resolved. We hope that our predictions stimulate further imaging or transmission experiments with a superlattice alone or with a superlattice much thicker than the substrate.

The formulation developed in this work could also be applied to the ballistic energy transport of phonons in materials with multidomain structures (with alternating electrical polarizations) like KDP. In the analysis of the heat transport in ferroelectric KDP (with

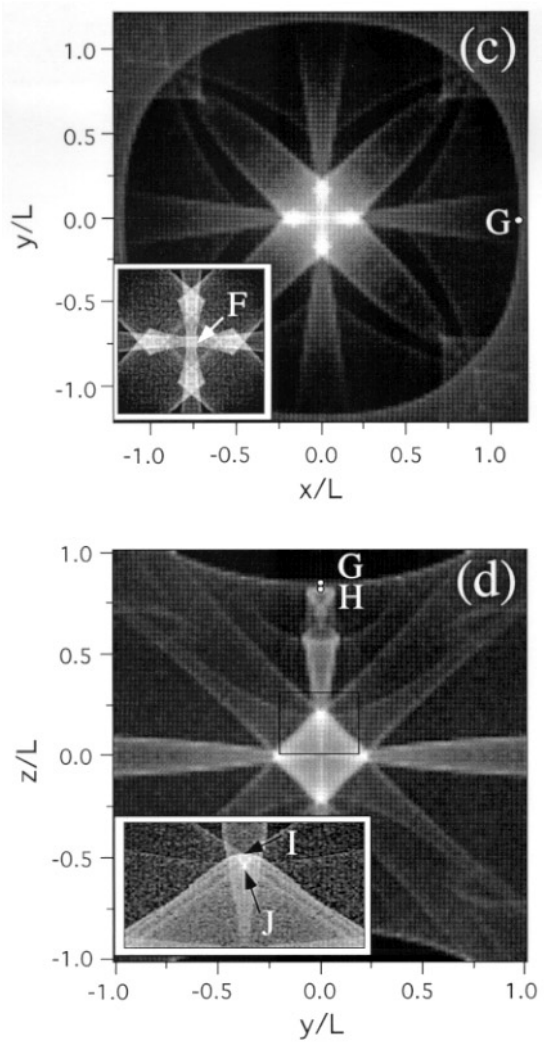

Figure 5. Continued

about 400 domain walls spaced 10 μm apart) a Monte Carlo method with transmissions and reflections of phonons at the domain boundaries was employed [9, 10]. This calculation is rather complicated because the transmission and reflection rates of phonons at a single interface depend on the phonon mode and incident angle. Moreover, the mode-conversions among three phonon polarizations happen at each interface. Our present formulation based on the Fourier-expansion method yields the phonon fields and the associated group velocities without invoking the transmission and reflection processes at layer interfaces. Thus the phonon images obtained automatically include the effects of phonon scatterings at the interfaces of the multilayered structures.

The images of phonons plotted in the present work do not contain any information about the phonon arrival times. The time-gated images should provide more detailed caustic structures depending on the phonon polarizations and also exhibit the predicted deformation of the group-velocity surfaces associated with the vanishing of the group-velocity component

in the growth direction. The study of the time-resolved phonon images in superlattices will appear elsewhere.

Acknowledgments

This work was supported in part by a Grant-in-Aid for Scientific Research from the Ministry of Education, Science and Culture of Japan (Grant No 09640385).

References

[1] Taylor B, Maris H and Elbaum C 1969 *Phys. Rev. Lett.* **23** 416
Taylor B, Maris H and Elbaum C 1971 *Phys. Rev.* B **3** 1462
[2] Northrop G A and Wolfe J P 1985 *Nonequilibrium Phonon Dynamics* (New York: Plenum) ch 5
[3] Baker A S Jr, Merz J L and Gossard A C 1978 *Phys. Rev.* B **17** 3181
[4] Tamura S and Wolfe J P 1987 *Phys. Rev.* B **35** 2528
[5] Hurley D C, Tamura S, Wolfe J P and Morkoc H 1987 *Phys. Rev. Lett.* **58** 2446
[6] Tamura S, Hurley D C and Wolfe J P 1988 *Phys. Rev.* B **38** 1427
[7] Capinski W S and Maris H J 1996 *Physica* B **219&220** 699
[8] Hyldgaard P and Mahan H J 1997 *Phys. Rev.* B **56** 10 754
[9] Weilert M A, Msall M E, Anderson A C and Wolfe J P 1993 *Phys. Rev. Lett.* **71** 735
[10] Weilert M A, Msall M E, Anderson A C and Wolfe J P 1993 *Z. Phys.* B **91** 179
[11] Tamura S and Harada T 1985 *Phys. Rev.* B **32** 5245
[12] Ramsbey M T, Wolfe J P and Tamura S 1988 *Z. Phys.* B **73** 167
[13] We used the elastic constants $C_A^{11} = 12.02$, $C_A^{12} = 5.70$ and $C_A^{44} = 5.89$ (in units of 10^{11} dyn cm^{-2}) and mass density $\rho_A = 3.76$ g cm^{-3} for AlAs, and $C_B^{11} = 11.88$, $C_B^{12} = 5.38$ and $C_B^{44} = 5.94$ (in units of 10^{11} dyn cm^{-2}) and mass density $\rho_B = 5.36$ g cm^{-3} for GaAs.